Available online at www.sciencedirect.com

SciVerse ScienceDirect

Acta Materialia 60 (2012) 2209–2218

Acta MATERIALIA

www.elsevier.com/locate/actamat

In situ TEM observation of grain annihilation in tricrystalline aluminum films

F. Mompiou [a,*], M. Legros [a], T. Radetic [b], U. Dahmen [b], D.S. Gianola [c], K.J. Hemker [d]

[a] CEMES-CNRS, 29, rue J. Marvig, 31055 Toulouse cedex 5, France
[b] University of California, Berkeley, Lawrence Berkeley Laboratory, National Center for Electron Microscopy, Berkeley, CA, USA
[c] Department of Materials Science and Engineering, University of Pennsylvania, Philadelphia, PA, USA
[d] Department of Mechanical Engineering, Johns Hopkins University, Baltimore, MD, USA

Received 17 October 2011; received in revised form 29 November 2011; accepted 5 December 2011

Abstract

Capillarity-driven grain boundary (GB) motion in Al tricrystalline thin films has been investigated by in situ transmission electron microscopy at intermediate temperatures. The GBs were observed to move erratically, with alternating periods of motion and stagnation, followed by rapid shrinkage of the grain and eventual annihilation accompanied by the emission of dislocations. The absence of measured deformation and grain rotation during the GB motion suggests that it is not associated with shear–migration coupling. This is in contrast to observations on the stress-driven motion of planar GBs. The present results can be interpreted by the absence of deformation associated with low internal applied stress or alternatively by a low shear–migration coupling factor. In both cases, a large amount of atomic shuffling is needed to account for the migration of grain boundaries.

Keywords: Grain boundary; Surface tension stress; Tricrystal; Shear–migration coupling; In situ TEM

1. Introduction

Molecular dynamics simulations suggest that grain boundary processes become predominant and are instrumental in relaxing the mechanical stresses applied to nanocrystalline materials, where normal dislocation activity is mitigated [1–3]. Among these processes, grain boundary migration has been shown to be particularly effective in nanocrystalline Al, even at room temperature [4–6], with this conclusion being supported by numerous simulation studies [7–10]. This process, in which grain boundary (GB) migration can effectively relax the stress by generating a permanent shear, is called shear-coupled grain boundary migration [11]. However, this process is far less well known than dislocation-based plasticity, where the shear carried by each dislocation line is equal to its Burgers vector. In shear-coupled GB migration, the shear is carried by the tilt component of the GB and is defined by a coupling factor β. Beta is usually defined as the shear produced parallel to the GB divided by the migration distance. This factor may depend on the GB character, as predicted by two models [10–13]. Experimental investigations have been carried out recently on shear-coupled GB migration in attempts to account for the amount of shear depending on the misorientation of tilt boundaries [14,15]. More recently, concomitant GB coupling and rotation have also been observed [16]. These studies focus principally on the motion of planar interfaces at high temperature under a moderate mechanical stress, mainly in bicrystals. Studies in polycrystals were recently initiated employing in situ transmission electron microscopy (TEM) and image correlation. These studies consistently show low coupling factors, despite large misorientation

* Corresponding author.
E-mail addresses: mompiou@cemes.fr (F. Mompiou), legros@cemes.fr (M. Legros), TRadetic@lbl.gov (T. Radetic), udahmen@lbl.gov (U. Dahmen), gianola@seas.upenn.edu (D.S. Gianola), hemker@jhu.edu (K.J. Hemker).

1359-6454/$36.00 © 2011 Acta Materialia Inc. Published by Elsevier Ltd. All rights reserved.
doi:10.1016/j.actamat.2011.12.013

angles [5,17,18]. In the past few years, the mechanism of GB sliding, a translation of grains along their GB, has been frequently invoked to describe deformation in nanocrystalline materials [1,19,20]. Experimental evidence suggests that GB rotation can be driven by a mechanical stress in nanocrystalline metals [21,22]. Grain rotation is also expected to occur during shear-coupled migration when curved GBs are involved [11]. However, despite the fact that capillarity-driven grain growth has been extensively studied theoretically and experimentally (see e.g. [23]), the notion that capillarity-driven grain boundary migration can be coupled to shear is generally overlooked. This question is of prime importance in order to better understand the GB migration processes in polycrystals. Indeed, in such materials where GBs are not stable and randomly distributed, GB migration under capillarity forces takes place as soon as either the temperature is elevated and/or GB migration is initiated under stress. Capillarity-driven GB migration at high temperature was earlier investigated by Babcock and Balluffi [24], who showed that GBs move erratically without producing shear deformation [25]. Babcock and Baluffi's studies were restricted to near Σ5 GBs; the current study provides an opportunity to consider a broader range of boundaries.

To study shear–migration coupling of curved GBs experimentally by in situ TEM, one can choose to activate as many GB shear-coupling processes as possible. This condition is met in nanocrystalline solids, but the GBs in these materials are extremely hard to characterize. Coarse-grained polycrystalline samples are much easier to characterize, but dislocation plasticity generally precedes coupled GB migration in these samples. Another option is to consider intermediate-sized grains of well-defined orientations that are produced by heteroepitaxial growth of metals on single crystal substrates. Gold and aluminum, for instance, have been deposited on Si, Ge and sapphire substrates with different orientations by vapor deposition [26,27]. The constraint imposed by the heteroepitaxial growth limits the number of different grain orientations by forming mazed multicrystal microstructures with many grains with a limited number (n) of allowed orientations [28]. For $n = 2$ and 3, this has led to highly controlled bi- or tricrystal morphologies, with fixed misorientation between grains, variable inclination of the GB plane and no or few triple junctions. Such morphologies have been used for the structural study of irrational GBs [29] and recently to investigate GB sliding [30]. Such systems where the misorientation between grains is precisely defined by the epitaxial conditions offer ideal candidates to test if a coupling exists when a given GB moves under a capillary force.

2. Experimental

Al tricrystals have been obtained by heteroepitaxy of Al on Si (1 1 1) at 280 °C. Details of the synthesis process can be found in [31]. At this temperature, Al crystallites grew mainly with the orientation relationship (0 0 1) Al ‖(1 1 1) Si and $[\bar{1}\,1\,0]$ Al ‖$[\bar{1}\,1\,0]$ Si. Because of the three equivalent ways of orienting a (0 0 1) Al on a (1 1 1) Si substrate, this resulted in three orientation variants. Columnar growth led to GBs that were perpendicular to the substrate and hence of pure tilt character. The film thickness was about 200 nm. To produce free-standing electron transparent films for subsequent straining, the substrate was removed by deep reactive ion etching. Thin strips of free-standing films were glued with epoxy onto copper grids. The assembly was heated with a GATAN high-temperature holder in a JEOL 2010 transmission electron microscope operating at 200 kV. Samples were heated up to between 250 and 400 °C. When recrystallization began, the temperature was maintained in order to observe GB motion. Video sequences were recorded using a MEGAVIEW III digital camera and a hard drive DVD recorder. Automatic crystallographic orientation mapping was performed using the Nanomegas ASTAR system [32] operating in a CM20FEG microscope.

3. Results

3.1. Microstructure

The typical microstructure of a (0 0 1) Al tricrystal (Fig. 1) is mainly composed of the three different variants Vi ($i = 1,2,3$) of the orientation relationship defined by the heteroepitaxial growth of (0 0 1) Al grains on a (1 1 1) Si substrate [31]. Wherever one of these variants $V1$ is dominant, it is called the matrix (M). The other two variants intertwine with the matrix and often form small grains ranging from a few tens of nm to several μm in size. Some of these exist as small "island" grains (I) (Fig. 1a). A selected area electron diffraction pattern taken along the ⟨0 0 1⟩ direction in a region marked in Fig. 1a shows that any two variants form a 30° (0 0 1) GB (Fig. 1b). A quantitative and systematic investigation of grain orientation was performed using the ASTAR system. Fig. 1c shows the orientation map perpendicular to the film plane (Oz direction). The majority of the grains are oriented in the ⟨0 0 1⟩ direction (red), corresponding to the common orientation direction of the three variants, normal to the film plane. A minority of small grains (labeled G) are oriented with the ⟨1 1 1⟩ direction (blue) normal to the film plane. Fig. 1d shows the in-plane orientation map along the Ox direction, highlighting the presence of the three (0 0 1) orientation variants. Except for the small fraction of (1 1 1) grains, the microstructure is that of a mazed tricrystal, and hence almost all the interfaces are 30° GBs. One of the three orientation variants is dominant and plays the role of the matrix phase (green), with the other two variants ($V2$ and $V3$) in the minority. Although there are triple junctions wherever three different color grains meet, several island grains that are fully surrounded by the matrix grain are also apparent. These are the island grains that were observed during in situ shrinkage.

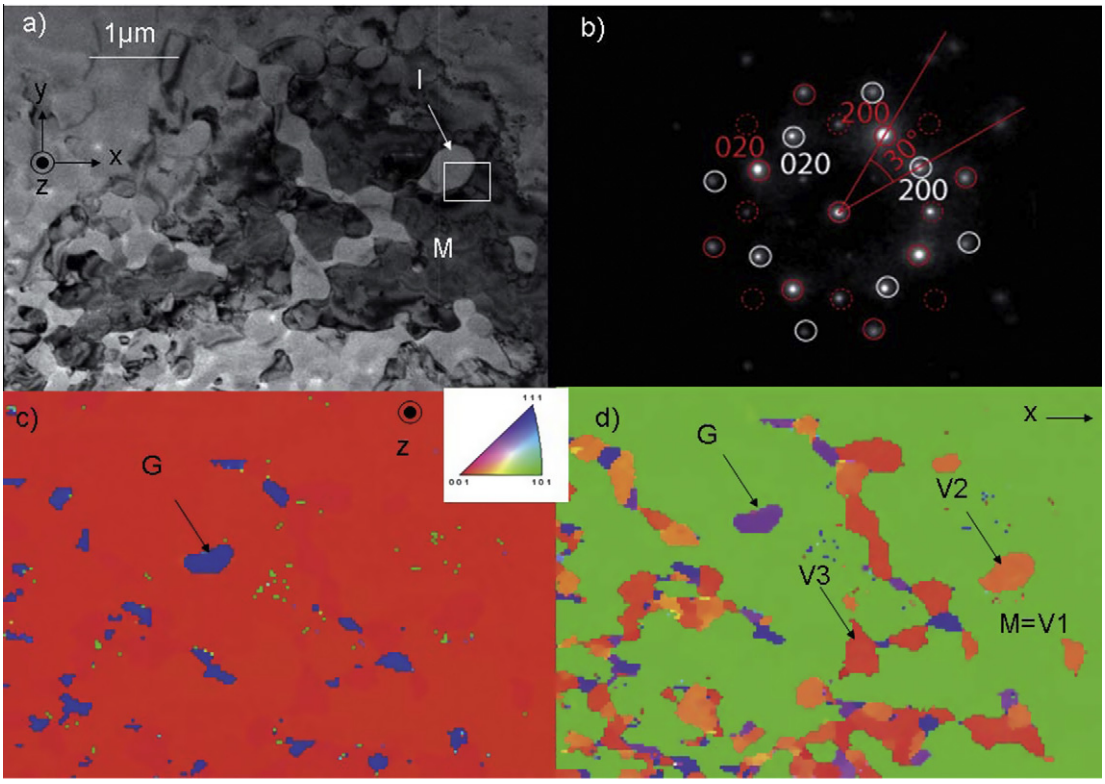

Fig. 1. (a) Bright-field image of the tricrystal microstructure showing the presence of different orientation variants. The dominant variant, marked (*M*) sometimes fully surrounds isolated grains such as that marked *I*. (b) Selected area electron diffraction (SAED) pattern taken in the area marked in (a) showing the 30° misorientation around the ⟨0 0 1⟩ direction normal to the sample (*Oz*). (c) Orientation map along the *Oz* direction highlighting the three (0 0 1) variants (red) and the small fraction of grains *G* in (1 1 1) orientation (blue). (d) Orientation map along the *Ox* direction showing the three (0 0 1) orientation variants *V*1, *V*2, *V*3 in red, orange and green and the small fraction of (1 1 1) grains *G* in purple. (For interpretation of the references to color in this figure legend, the reader is referred to the web version of this article.)

3.2. In situ TEM observations

3.2.1. Grain shrinkage

Fig. 2 shows the shrinkage of a 500 nm island grain during in situ heating at 350 °C. Because the sample is tilted with respect to the electron beam, the grain appears like an inclined cylindrical tube, and the GB looks like a ribbon with fringe contrast typical for two-beam diffracting conditions. An array of interfacial dislocations is clearly visible. As the grain shrinks, the dislocations remain in the GB and thus move closer together. Note that the rate of observed GB motion accelerates greatly during the latter stage of the process. The shrinkage sequence from (a) to (g) takes 269 s, while the remaining grain disappears completely in the last second. This final step is associated with a burst of dislocations, as seen in Fig. 2. During the shrinking process, slip traces (noted *tr*) are seen accompanying the GB motion (Fig. 2a–c). This is probably due to a trailed dislocation (*d*), visible in Fig. 2d when it is released. From then on (Fig. 2d–h), *d* is immobile and slip traces are no longer created. From this figure it is also apparent that the grain is a cylinder with a narrow waist in the center of the foil. This is typical for a catenoid shape, which minimizes the surface of cylindrical grains in thin films [33].

Fig. 3 shows the shrinkage of the grain labeled *G*1, the grain *G*2 being immobile. In this sequence dislocation emission during and at the end of shrinkage is more clearly visible. During the shrinkage, it is interesting to note that, because the upper part of the GB is less curved, it is almost immobile. Due to the shrinkage, the curvature of the moving part increases, becoming acute on the right (labeled *A* in Fig. 3c). The presence of an extinction contour at *A* indicates a stress concentration in this area. Dislocations (*d*) emitted from this point can be seen in Fig. 3c. In total, 20 dislocations were emitted during the collapse of *G*1.

3.2.2. Grain shrinkage dynamics

The grain shrinkage process appears to be irregular, alternating between long periods of motion at slow speed (less than a few nanometers per second) and strong acceleration at the end, reaching more than 500 nm s^{-1}. The variation in the diameter *D* of another grain (not shown here) as a function of time is shown in Fig. 4 (crosses). This can be compared with a classical curvature-driven GB motion, for which the GB velocity is proportional to curvature. It yields the following differential equation for the grain diameter:

$$\frac{dD}{dt} = \frac{M\gamma}{D} \tag{1}$$

where *M* is the GB mobility and γ is the surface tension. The integration of Eq. (1) leads to:

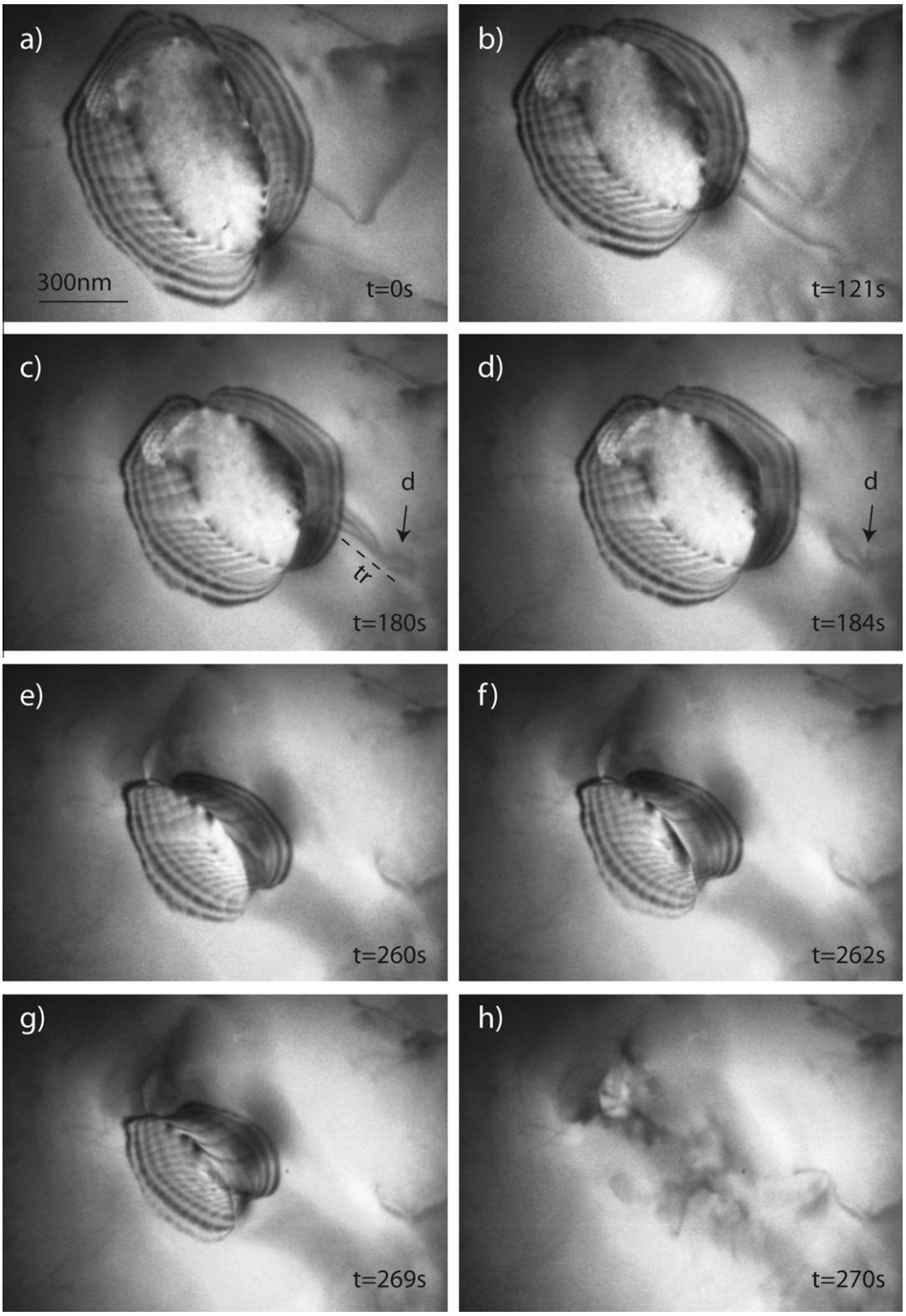

Fig. 2. Shrinking sequence of an island grain viewed at an angle to the foil surface. Note the emission of a dislocation d from the shrinking grain at $t = 180$ s (c).

$$D(t) = D_0\sqrt{1 - \frac{t - t_a}{t_0}} \qquad (2)$$

where t_a is the time at which the GB starts to move and $t_0 = \frac{2M\gamma}{D_0^2}$ is a time constant corresponding to the shrinking

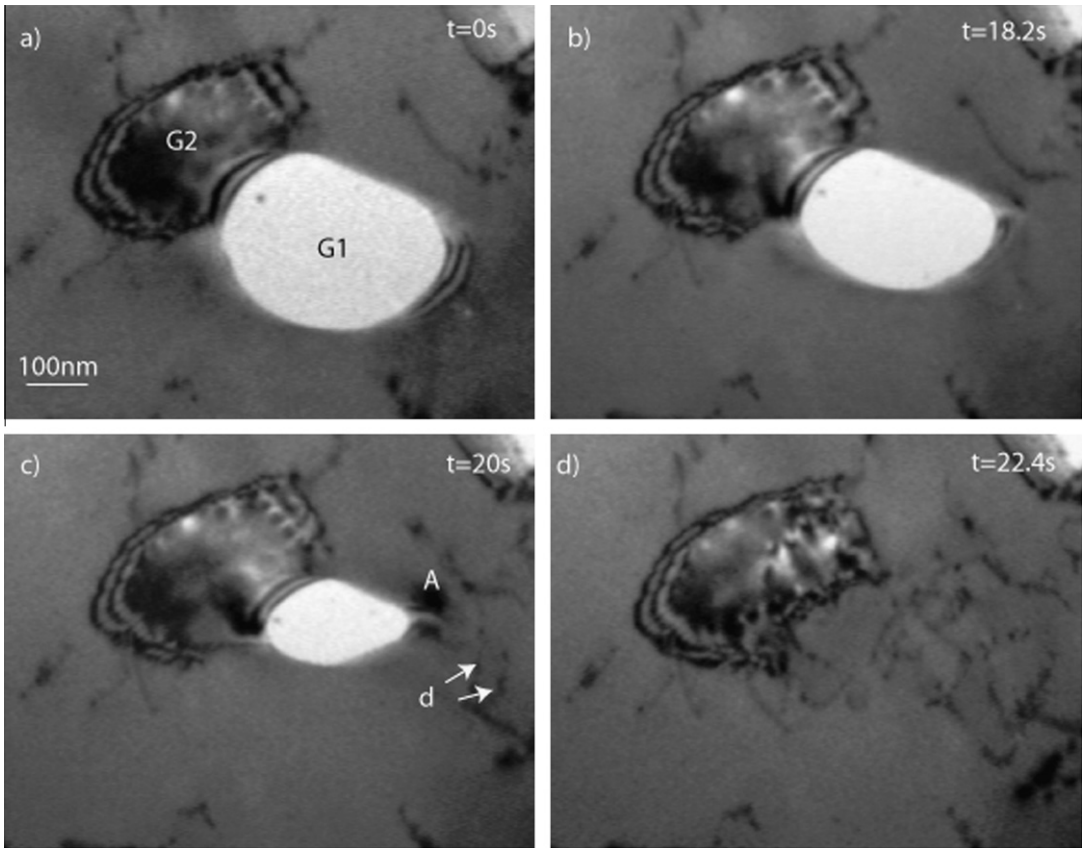

Fig. 3. Snapshots showing the asymmetrical shrinking of grain $G1$. Note the emission of dislocations (d) at A (c) before the final dislocation burst (d).

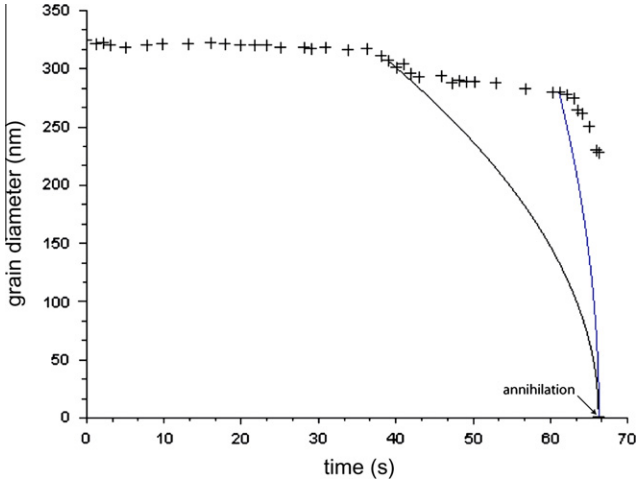

Fig. 4. The evolution of the grain diameter D with time, showing a long period of slow motion and a sudden acceleration at the end of the shrinkage. The two curves show the expected curvature-driven behavior for two different initial conditions.

time. The data in Fig. 4 cannot be fitted with a single time constant. Two curves corresponding to two different values of t_a are shown in Fig. 4: $t_a = 39$ s for the black curve and $t_a = 61$ s for the blue one, respectively. It can be seen that sections of the data appear to follow classic curvature-driven migration even though the full curve does not.

3.2.3. Dislocation activity during shrinkage

Island grains are usually defect free, but both the matrix and the interface contain dislocations. Most of these dislocations form subgrain boundaries in the matrix and extrinsic dislocations form arrays in the interface. Because such dislocations can move or be emitted from the interface during the shrinking process, as shown in Fig. 2, we thought it important to further characterize these dislocations and investigate the dislocation mechanisms.

In Fig. 5 a subgrain boundary can be seen to be attached to the right part of an island grain. The constituent dislocations were characterized using the $\vec{g} \cdot \vec{b} = 0$ extinction rule in bright-field pictures ($\vec{g}$ being the diffraction vector and $\vec{b}$ the dislocation Burgers vector). Their Burgers vector is perpendicular to both the rotation axis and the subgrain boundary plane. The dislocation lines lie along the $\langle 0\,0\,1 \rangle$rotation axis. Thus, the subgrain boundaries correspond to a small-angle tilt grain boundary with a misorientation around the rotation axis. Although extrinsic dislocations in the GBs cannot simply be determined using extinction rules as for lattice dislocations, we can reasonably assume that these dislocations come from the matrix and are trapped in the GB. They are thus of the same type as those composing the subgrain boundaries. This assumption is consistent with the expected black/white contrast along the dislocation line according to the Marukawa and Matsubara contrast rules [34,35].

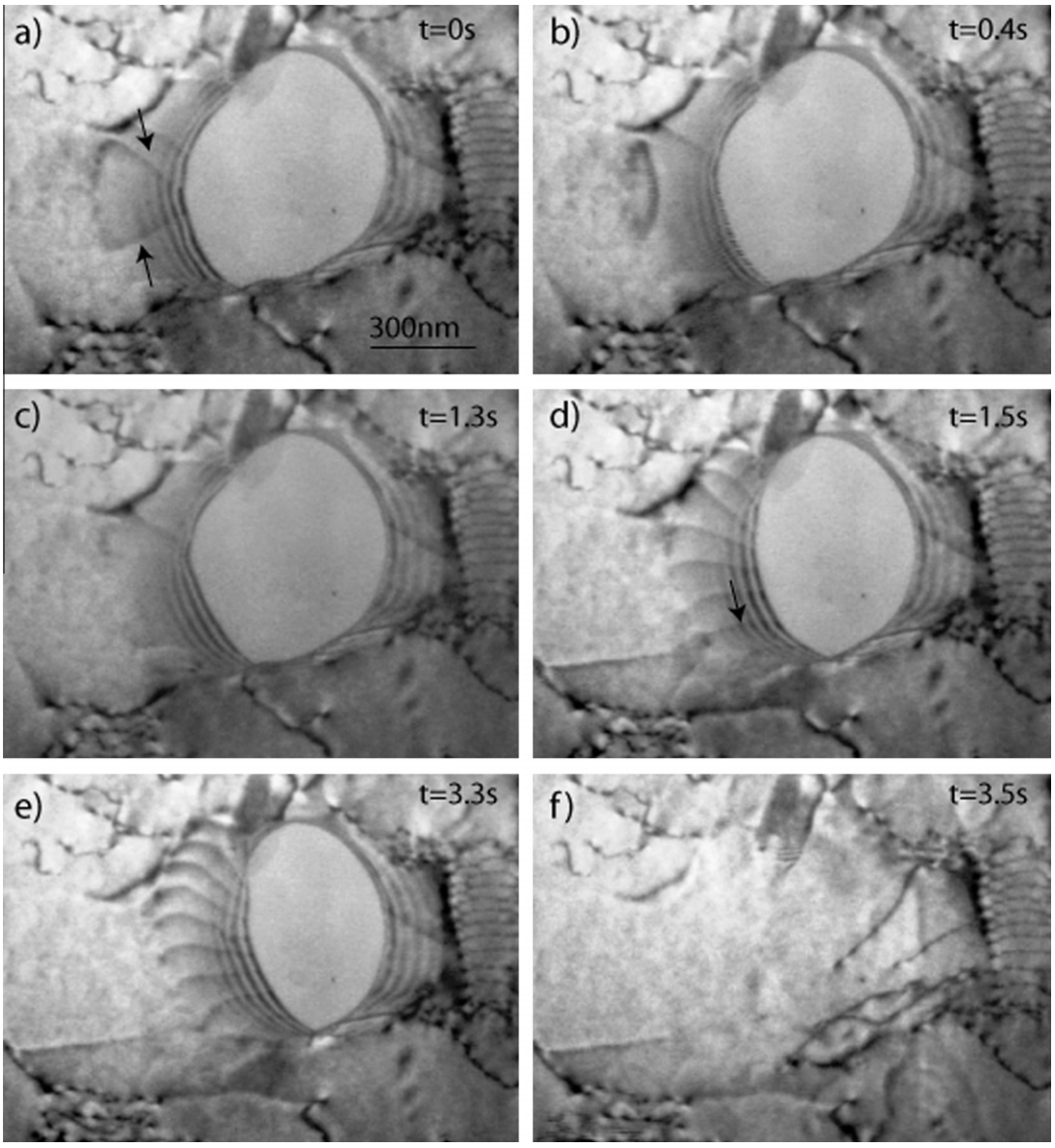

Fig. 5. Annihilation (a and b), nucleation (d) and motion (e) of dislocations in the GB during a shrinking process.

The concomitant motion of these dislocations with the GB migration has been frequently observed, as shown, for instance, in Fig. 5 during a much more asymmetric grain shrinkage. In Fig. 5a, two dislocation segments (see arrows) glide in opposite directions along the GB. The annihilation starts when the two segments meet (Fig. 5b and c). When the shrinkage of the grain begins in Fig. 5d, seven interfacial dislocations are nucleated in the GB. A trace of dislocation motion can also be seen in the matrix, in the lower left part of the image. At this time, the left part of the GB is moving at its highest speed (around 400 nm s^{-1}), while the other parts remain fixed. Subsequently (Fig. 5e), the left part of the GB keeps moving erratically. No dislocations are emitted in this process, but they seem to be trailed by the GB. The fact that they bend more during the shrinkage (Fig. 5d and e) indicates that the lower and upper parts of the GB with respect to the foil surfaces do not move at the same speed. The grain eventually shrinks very abruptly within a time period of 0.2 s (Fig. 5f). As seen before, a burst of dislocations is observed at the point of grain annihilation, although many of the emitted dislocations are invisible due to the visibility criteria under the diffraction contrast conditions.

Fig. 6 shows the shrinkage sequence of an elongated grain. The two acute ends of the grain are located in the vicinity of subgrain boundary (SGB) tips. As the elongated grain shrinks, the dislocations (noted *d* in Fig. 6b) seem to be nucleated at the left tip, leading to an extension of the SGB. The grain finally disappears, leaving a single SGB. Some dislocations (*d*) are also emitted in the matrix (Fig. 6c). This phenomenon supports Li's suggestion [36] that SGBs can grow when a "Y" junction is formed. In our experiment, the three branches of the "Y" are formed by three SGBs. The lower branch has a higher misorienta-

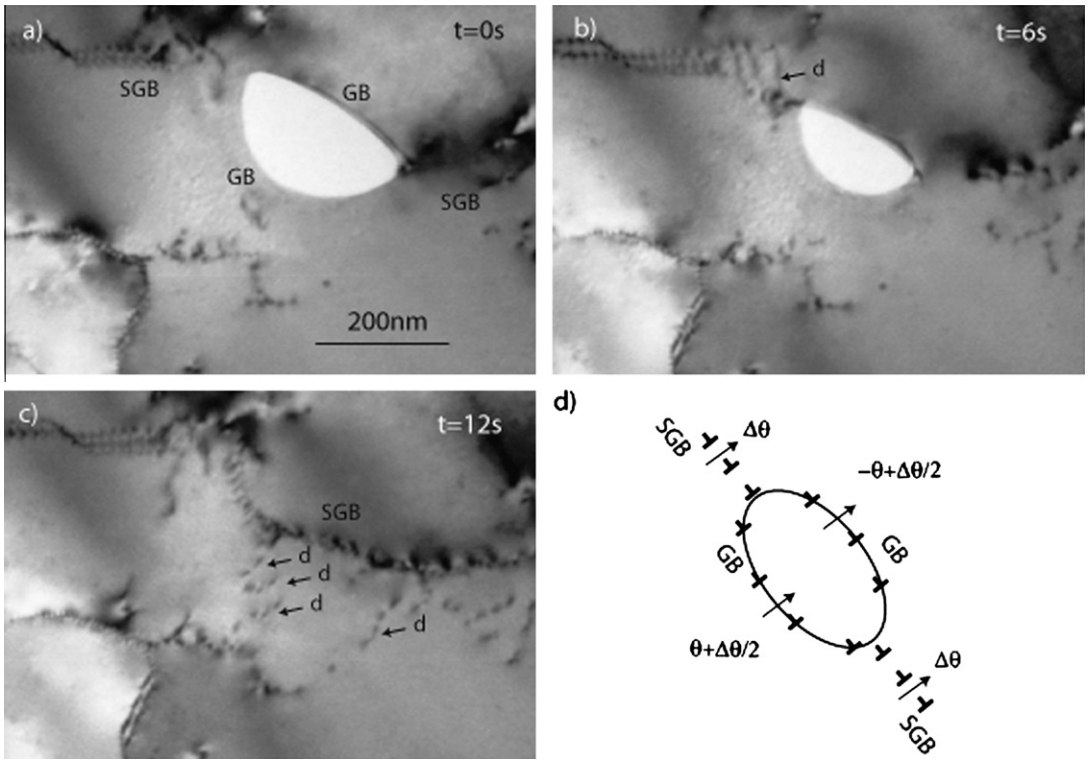

Fig. 6. GB zipping due to the presence of two subgrain boundaries (SGB) in the vicinity of an isolated grain. Misorientations across SGBs ($\Delta\theta$), GBs (θ) and the dislocation content are shown in (d).

tion angle (i.e. a smaller dislocation spacing) than the other two branches. It can be shown that dislocations in the two upper branches are attracted by the lower branch, and will find a stable position right above the lower branch. Under such conditions, and assuming dislocations are able to rearrange to form an SGB, the "Y" junction would move upward (Fig. 6). Despite the fact that dislocations here are located in a GB, they still interact with the elastic stress field of a nearby SGB. Thus, the structure shown in Fig. 6 can be interpreted as a double "Y" junction, as schematically described in Fig. 6d. The misorientation angle of a tilt GB can be calculated via the classical equation

$$\Delta\theta = \arctan\frac{b}{2h} \tag{3}$$

where h is the distance between dislocations. This yields a misorientation angle across the SGB $\Delta\theta_{SGB} = 1.2°$, which is approximately twice the misorientation across the two GBs calculated from the spacing of the extrinsic dislocations. This is in agreement with the expected geometry of the "Y" junction, as shown in Fig. 6d (note the misorientation angles indicated by arrows at the interfaces in Fig. 6). As the two junctions move toward each other, they yield to a zipping of the grain. It is then expected that the shrinkage of the grain should be enhanced by this zipping of the junction.

3.2.4. Quantification of deformation incurred during GB migration

In order to investigate whether GB motion driven by capillarity effects is coupled to plastic strain, an estimate of the local deformation was performed. Fig. 7 shows an image correlation analysis to estimate the deformation mapping during an in situ TEM sequence, in which we have decorated the sample surface with 10 nm gold nanoparticles acting as fixed markers for tracking (labeled X). Three of these markers, $X1$, $X2$ and $X3$, are located on the surface of the shrinking grain; the other one, $X4$, is on the surface of the matrix. A difference image between the initial state where the grain began to shrink and the final one where the grain has disappeared is shown in Fig. 7d. The contrast of the difference image is a metric for correlation between the initial and final states; low contrast is high correlation, while high contrast represents a significant change. Focusing on the contrast obtained from our reference marker $X4$ in a region away from the shrinking grain, it is apparent that the correlation is high, meaning that little or no motion of the surrounding matrix is observed. The three markers inside the grain also display very little motion, as indicated by the uniform gray contrast at the marker positions, suggesting that no deformation is associated with this GB migration. With a precision of one pixel at the marker position, it can be said that the apparent coupling factor perpendicular to the viewing direction is less than $s_m/m_3 \approx 2.3$ nm/190 nm $\approx 1.2\%$ (m_3 is the maximum measured migration distance, i.e. the distance between the GB at its initial position and marker $X3$).

3.2.5. Measurements of grain rotation

To further investigate any potential deformation induced by GB migration, measurements of grain rotation

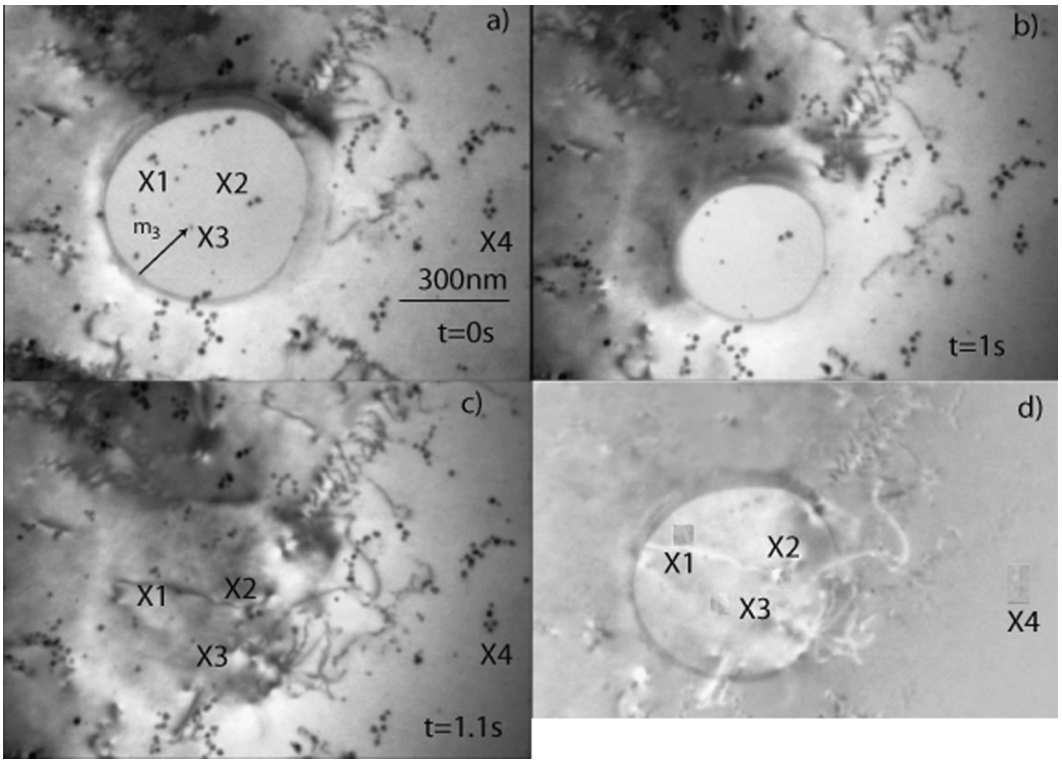

Fig. 7. (a–c) Shrinkage sequence observed in a sample coated with gold nanoparticles. Three of these particles (marked *X*1, *X*2 and *X*3) located inside the shrinking grain and one (*X*4) outside served as markers to probe the deformation. (d) Difference image of (a–c) obtained by superimposing the *X*4 markers. Note the absence of marker displacements inside the grain.

were conducted during grain shrinkage. Because the GB is curved, if a shear parallel to the GB plane and perpendicular to the tilt axis exists, we should observe a rotation of the planes parallel to the tilt axis. In order to test for such a rotation, we followed a grain shrinkage in the reciprocal space, using diffraction conditions along the [0 0 1] zone axis (i.e. parallel to the tilt axis). In the initial configuration (Fig. 8a and c), the diffraction pattern in the [0 0 1] zone axis condition with a selected area aperture over both the grain G and the matrix (Fig. 8a) shows the two [0 0 1] reciprocal lattices rotated by 30° (Fig. 8c). As the grain shrinks, the diffraction pattern does not evolve (Fig. 8d). At $t = 7.5$ s, the grain has disappeared, thus the diffraction pattern from just the matrix remains (Fig. 8b and e). Based on image correlation of the two patterns taken just before grain shrinkage, we can estimate that the grain did not rotate more than 0.5° around the tilt axis. The theoretical variation of the misorientation angle θ with migration distance has been extensively discussed in Ref. [11] for the case of a circular GB subjected to coupling or sliding. For the case of pure coupling and for a constant coupling factor,[1] this variation can be deduced geometrically as follows. Consider a grain of initial radius R_0. For a given radius $r = R_0 - m$, m being the migration distance, a small decrease dr will produce a grain rotation $d\alpha$ and a tangential shear ds following the relations (see Fig. 8f):

$$r d\alpha \approx ds \tag{4}$$

and

$$\beta = \frac{ds}{dr} \tag{5}$$

Combining Eqs. (4) and (5) and integrating leads to:

$$\alpha = \beta \ln \frac{R_0 - m}{R_0} \tag{6}$$

The misorientation $\theta = \theta_0 \pm \alpha$ (θ_0 being the initial misorientation) will increase or decrease depending on the grain rotation sign. For a migrating distance $m \approx 0.5 R_0$, this leads to $\alpha = 40\beta$ (in degree). With a resolution of 0.5° for the experimental value of θ, this leads to an upper bound for $\beta \approx 2\%$, in agreement with the results in Section 3.2.4.

4. Discussion

Several salient features of grain shrinkage processes under capilarity forces have been observed in this work:

1. the GB motion is jerky,
2. the GB accelerates in the last stage of annihilation,
3. there is no apparent shear–migration coupling and no grain rotation, and
4. dislocation emission occurs during and at the end of the shrinkage process.

[1] This assumption is valid only when one coupling mode operates, i.e. when the misorientation variation is small.

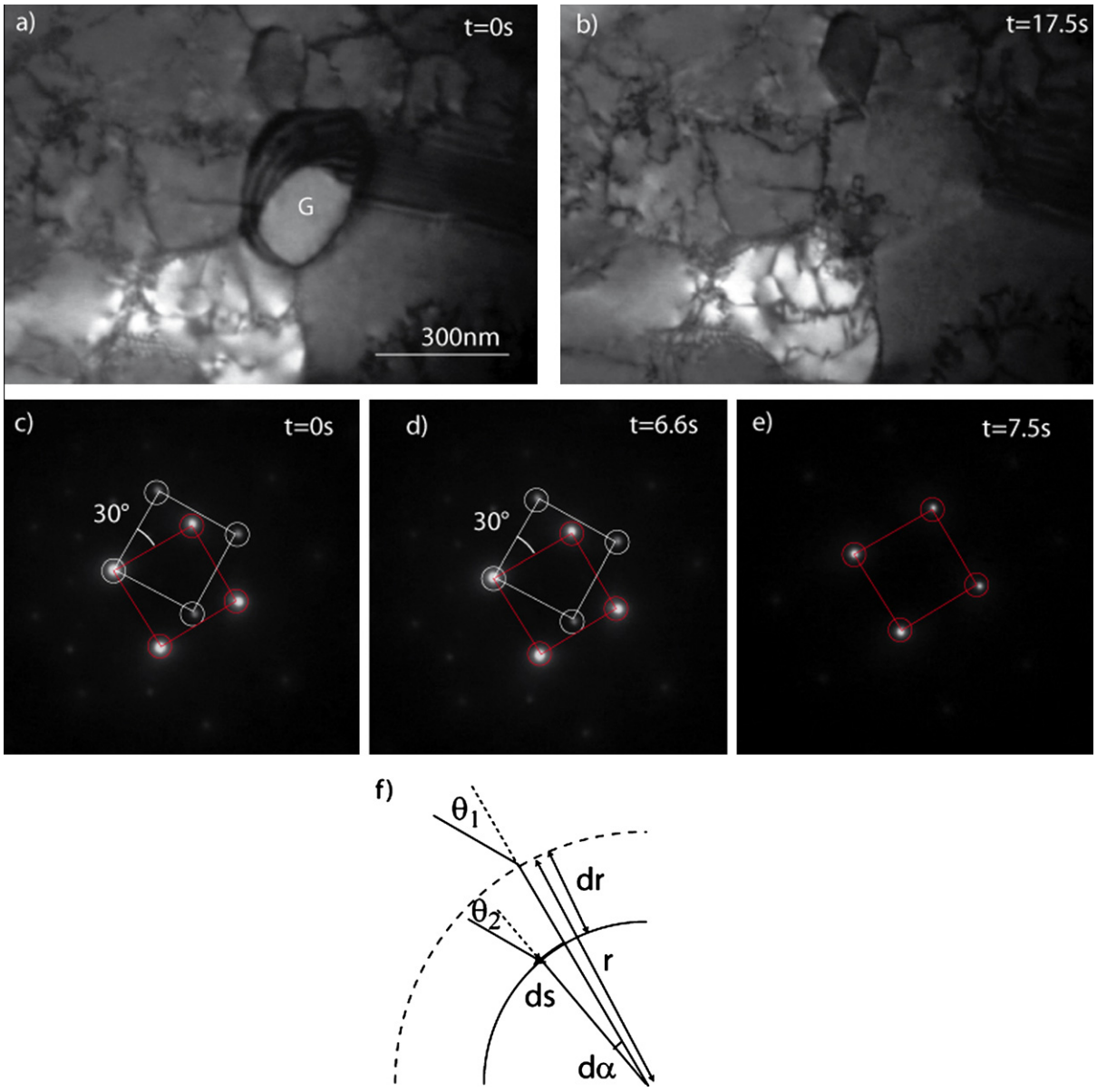

Fig. 8. (a and b) Two snapshots taken before and after the grain G has shrunk. The evolution of the (0 0 1) zone axis SAED patterns (c–e) taken for both variants shows no rotation of the grain during the shrinkage. A shear–migration coupled process in a curved GB of radius r (e) should lead to a grain rotation of angle $d\alpha$, which varies with the coupling factor $\beta = ds/dr$ (f).

Points 1 and 3 are in agreement with the conclusions drawn by Babcock and Baluffi [24] indicating that capillarity forces do not couple with the GB motion. Babcock and Baluffi suggested that migration occurs in that case by pure shuffling. In this mechanism, the GB migrates by the conservative motion of pure step involving a limited motion of atoms. In the present case, where the GB is far from a low index coincident site lattice (CSL) condition, pure steps cannot exist. However, extrinsic interfacial defects with a step and dislocation character, i.e. disconnections according to Ref. [37], may be present. Because of their step character, their lateral motion in the GB causes the rearrangement of atoms from one grain to another. Such defects are suspected to have nucleated from a spiral source with a lattice dislocation as a fixed arm [38]. This kind of source has been observed in a non-planar non-coincident GB in Al [39]. Fig. 9 shows extrinsic dislocations distributed concentrically around a source S not visible here under this diffraction condition. The inset of Fig. 9 shows the same region under different diffraction conditions. A lattice dislocation intersecting the GB near S can be seen, supporting the idea of a spiral source. The concomitant motion of such defects and GB migration (Fig. 5) suggests that dislocation mechanisms are also active. Other extrinsic dislocations originating from the matrix and trapped in the GB have also been frequently observed (cf. Fig. 2, for instance).

However, the sole motion of these dislocations cannot explain the GB migration; if it could, a shape change or

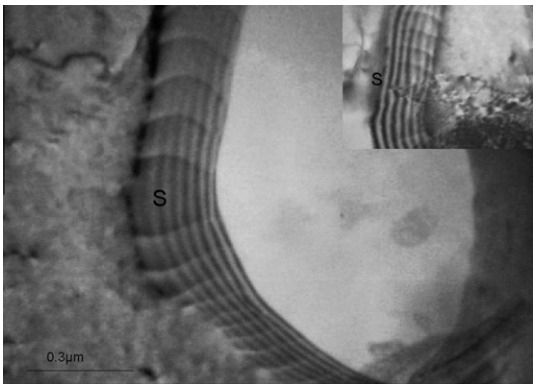

Fig. 9. Observation of extrinsic dislocations emitted from a spiral source S. The fixed arm of the source, shown in the inset under different diffraction conditions, is a lattice dislocation intersecting the GB.

GB rotation would be expected. This indicates that interfacial dislocations are not geometrically necessary dislocations and thus their motion does not correlate with shear. Indeed, because the GB is curved, the atomic environment along the GB varies from place to place. In some restricted areas, the GB structure can sustain extrinsic dislocations, but in most parts, the GBs have to migrate by transferring atoms directly from one grain to another. Such a mechanism, coined "uncorrelated atomic shuffling" by Sutton and Baluffi [38], does not produce strain or rotation. In the area containing dislocations, a local strain or rotation can be produced. For instance, in Fig. 2, the distance between extrinsic dislocations in the lower left part of the GB decreases from 50 nm (Fig. 2a) to 35 nm (Fig. 2g) due to the reduction in the GB area. This yields a small local increase in the misorientation of 0.16°. This grain rotation can be compensated by emitting one or several dislocations in the matrix. In the general case, the constraint geometry of the shrinking grain, i.e. the absence of a triple junction and adjacent grain, prevent the deformation from being relaxed. Because the produced strain progressively increases as the grain shrinks, a relaxation mechanism has to operate before the interface disappears.

5. Conclusions

The annihilation of sub-micron grains in Al tricrystalline films has been monitored at intermediate temperature using in situ TEM. The driving force of the associated grain boundary motion is the reduction of the surface energy contained in boundaries. The annihilation of smaller Al grains (100–500 nm) in a larger Al matrix occurs via the jerky migration of opposite grain boundaries and the eventual nucleation of dislocations. By combining fiducial markers on the surface and image correlation of the before and after annihilation states, we showed that the GB migration leads to no permanent deformation, or to a deformation that is below the threshold of this method. When monitored under diffraction mode, annihilating grains also displayed a total absence of rotation. We hypothesize that this shrinkage without deformation operates mostly via uncorrelated atomic shuffling and to a lesser extent via the motion of extrinsic GB dislocations. It is also explained that, in the absence of applied stress, shear migration coupling does not occur, or takes place with a very low coupling factor, that we were unable to measure.

Acknowledgement

The authors acknowledge S. Mornet (ICMCB-CNRS, Bordeaux) for providing gold nanoparticles.

References

[1] Van Swygenhoven H, Derlet P. Phys Rev B 2001;64:224105.
[2] Yamakov V, Wolf D, Phillpot S, Gleiter H. Acta Mater 2002;50:61–73.
[3] Haslam A, Moldovan D, Yamakov V, Wolf D, Phillpot S, Gleiter H. Acta Mater 2003;51:2097–112.
[4] Gianola D, Van Petegem S, Legros M, Brandstetter S, Van Swygenhoven H, Hemker K. Acta Mater 2006;54:2253–63.
[5] Legros M, Gianola D, Hemker K. Acta Mater 2008;56:3380–93.
[6] Rupert T, Gianola D, Gan Y, Hemker K. Science 2009;326:1686–90.
[7] Wan L, Wang S. Phys Rev B 2010;82:214112.
[8] Shiga M, Shinoda W. Phys Rev B 2004;70:054102.
[9] Zhang H, Srolovitz D. Acta Mater 2006;54:623–33.
[10] Cahn J, Mishin Y, Suzuki A. Acta Mater 2006;54:4953–75.
[11] Cahn J, Taylor J. Acta Mater 2004;52:4887–98.
[12] Caillard D, Legros M, Mompiou F. Acta Mater 2009;57:2390–402.
[13] Mompiou F, Legros M, Caillard D. Acta Mater 2010;58:3676–89.
[14] Molodov D, Ivanov V, Gottstein G. Acta Mater 2007;55:1843–8.
[15] Gorkaya T, Molodov D, Gottstein G. Acta Mater 2009;57(18):5396–405.
[16] Gorkaya T, Molodov KD, Molodov DA, Gottstein G. Acta Mater 2011;59:5674–80.
[17] Mompiou F, Caillard D, Legros M. Acta Mater 2009;57:2198–209.
[18] Mompiou F, Legros M, Caillard D. J Mater Sci 2011;46:4308–13.
[19] Markmann J, Bunzel P, Rsner H, Liu K, Padmanabhan K, Birringer R, et al. Scripta Mater 2003;49:637–44.
[20] Schiotz J, Di Tolla F, Jacobsen K. Nature 1998;391:561–3.
[21] Harris K, Singh V, King A. Acta Mater 1998;46:2623–33.
[22] Liu P, Mao S, Wang L, Han X, Zhang Z. Scripta Mater 2011;64:343–6.
[23] Thompson C. Ann Rev Mater Sci 2000;30:159–90.
[24] Babcock S, Balluffi R. Acta Metall 1989;37:2357–65.
[25] Babcock S, Balluffi R. Acta Metall 1989;37:2367–76.
[26] Westmacott K, Hinderberger S, Dahmen U. Philos Mag A 2001;81:1547–78.
[27] Dehm G, Inkson B, Wagner T. Acta Mater 2002;50:5021–32.
[28] U. Dahmen, T. Radetic, Proc. 1er Colloque 3M (2007) 39–45.
[29] Medlin D, Cohen D, Pond R. Philos Mag Lett 2003;83:223–32.
[30] Lancon F, Ye J, Caliste D, Radetic T, Minor AM, Dahmen U. Nano Lett 2010;10:695–700.
[31] Thangaraj N, Westmacott K, Dahmen U. Appl Phys Lett 1992;61:913–5.
[32] Moeck P, Rouvimov S, Rauch EF, Veron M, Kirmse H, Hausler I, et al. Cryst Res Technol 2011;46:589–606.
[33] Mullins WW. Acta Metall 1958;6:414–27.
[34] Marukawa K, Matsubara Y. Trans Jap Inst Metals 1979;20:560–8.
[35] Couzinie J, Decamps B, Priester L. Int J Plast 2005;21:759–75.
[36] Li JCM. Acta Metall 1960;8:563–74.
[37] Pond R. Dislocation in solids, vol. 8(38). Elsevier; 1989.
[38] Sutton A, Balluffi R. Interfaces in crysalline materials. Oxford University Press; 1995.
[39] Dingley D, Pond R. Acta Metall 1979;27:667–82.